

# Molecular BioSystems

Accepted Manuscript



This is an *Accepted Manuscript*, which has been through the Royal Society of Chemistry peer review process and has been accepted for publication.

*Accepted Manuscripts* are published online shortly after acceptance, before technical editing, formatting and proof reading. Using this free service, authors can make their results available to the community, in citable form, before we publish the edited article. We will replace this *Accepted Manuscript* with the edited and formatted *Advance Article* as soon as it is available.

You can find more information about *Accepted Manuscripts* in the [Information for Authors](#).

Please note that technical editing may introduce minor changes to the text and/or graphics, which may alter content. The journal's standard [Terms & Conditions](#) and the [Ethical guidelines](#) still apply. In no event shall the Royal Society of Chemistry be held responsible for any errors or omissions in this *Accepted Manuscript* or any consequences arising from the use of any information it contains.



[www.rsc.org/molecularbiosystems](http://www.rsc.org/molecularbiosystems)

higher cytotoxicity of TQ towards MCF-7 breast cancer cells in comparison to normal cells indicate the potential of TQ to be an anticancer drug.

### 1. Introduction:

The process for acetylation and deacetylation of histones presents the two sides of the same coin, regulating the activity of chromatin and plethora of other cellular activities. Several studies have envisaged the role of HDACs in development and progression of human cancer. These HDACs undergo an active participation in gene silencing in context with cell cycle regulation, differentiation, apoptosis, angiogenesis, invasion, adhesion and metastasis<sup>1, 2</sup>. Thus, the inhibitors against these enzymes are emerging as promising class of anticancer agents that have been tested for the treatment of multifarious malignancies. As of now, romidepsin and vorinostat are recognized as US Food and Drug Administration approved drugs for cutaneous T-cell lymphoma, while romidepsin alone for relapsed peripheral T-cell lymphoma. Indeed, most of the HDAC inhibitors (HDACi) are still under different phases of preclinical and clinical investigations against various relapsed and refractory lymphoid malignancies, myeloid leukemia, and solid tumors<sup>3</sup>.

Unfortunately, higher clinical dose of synthetic HDACi induces extensive DNA damage and impair DNA breaks repair leading to undesired cytotoxicity<sup>4</sup>. The most common toxicities evinced by such HDACi include fatigue, diarrhea and nausea, while cardiac toxicity is most prevalent among all. Nevertheless, the usual doses of synthetic HDACi might also exert adverse effects including vomiting, anorexia, dehydration, myelosuppression, thrombocytopenia, anemia and pulmonary embolism<sup>5</sup>. Besides these inhibitors are expensive and have narrow specificity. This brings dietary chemopreventive agents into lime light, with widespread availability, possible incorporation in diets and negligible toxic effects. Of these, some bioactive phytochemicals have potential to alter the anomalous expression of cancer

related genes by modulating epigenetic events. For example, curcumin from turmeric, epigallocatechin-3-gallate (EGCG) from green tea, procyanidine B2 from grape seeds and sulforaphane (SFN) from broccoli are effective phytoconstituents to alter the aberrant DNA methylation and histone modification in different malignancy<sup>6,7</sup>.

Experimental evidences suggest that diallyl disulfide and SFN increase p21waf1/cip1 expression in human colon cancer cells by inhibiting HDACs<sup>2, 8</sup>. Likewise, polyphenols are one of the important bioactive dietary components having chemopreventive and therapeutic potential against various diseases. Among them, thymoquinone (2-isopropyl-5-methyl-1,4-benzoquinone) (TQ), the active constituent of *Nigella sativa* (Black cumin) holds potential significance. Numerous cell line and animal experiments have demonstrated the anti-inflammatory and chemopreventive nature of TQ in different diseases. It has been reported to have antineoplastic activities in multiple forms of cancer; including breast cancer, osteosarcoma, prostate cancer, myeloblastic leukemia, squamous cell carcinoma and gastric carcinoma<sup>9-12</sup>. Additionally, it has also been demonstrated to elicit antitumor activity in mouse tumor models xenografted with breast<sup>13</sup>, colon<sup>14</sup> and prostate cancer<sup>15</sup>. In view of the above perspectives, we intended to investigate about the dietary supplement TQ. Several lines of study have contributed to explain the anticancer effects of TQ, which is attributed via induction of peroxisome proliferator-activated receptor gamma, PTEN expression, p53-dependent and independent apoptosis<sup>9, 10, 16</sup>.

HDAC inhibitors have been reported to upregulate the expression of multiple genes, including p21waf1/cip1 gene and GADD45, associated with inhibition of proliferation, induction of differentiation and/or apoptosis of transformed cells<sup>2, 8, 17</sup>. Remarkably, TQ have also been demonstrated to induce apoptosis via overexpression of p21waf1/cip1 gene in doxorubicin resistant breast cancer cells and osteosarcoma cells<sup>10, 16</sup>. In view of this, we sought to investigate the HDAC inhibition activity of TQ. Furthermore, chemical and

structural insights of HDAC active site and the information on existing HDAC inhibitors compelled us to proclaim the inhibitory role of TQ against HDACs. Hence, in the present study, we have attempted to illuminate the elementary interactions of TQ with HDAC by *in-silico* approach which is comprehended by *in-vitro* cell culture study to interrogate the consequence of such interactions. We also aimed to compare the cytotoxic nature of TQ towards breast cancer cells and normal keratinocytes to establish its toxicity to cancer cell lines compared to normal cell lines.

## **2. Materials and Methods:**

### ***2.1. In-silico approach to study inter-molecular interaction between Thymoquinone and HDACs:***

#### **2.1.1. Multiple Sequence Alignment**

Multiple sequence alignment was carried out to study the homology of HDAC1 and HDAC2 protein with the model organism *Aquifex aeolicus*. Amino acid sequences for respective proteins were retrieved from Uniprot database bearing the accession number Q13547, Q92769 and O67135. The sequence alignment was carried out by the web based application of CLUSTALW. The analysis was based upon BLOSUM substitution matrix with gap penalty of 10 and extension of 0.2.

#### **2.1.2. Structure Preparation for protein and ligand**

The X-ray crystallographic structure of human HDAC1 and HDAC2 (PDB id: 4BKX, 3MAX) co-crystallized with  $Zn^{2+}$  and other ligand molecules at resolutions of 3.0 and 2.05Å respectively, was retrieved from RCSB Protein Data Bank<sup>18</sup>. The hetero-atoms other than zinc ion (other than active site) were edited using chimera software. The hydrogen atoms were added to calculate initial partial Gasteiger charge calculation; however the non-polar hydrogens were merged later on. The structures of both the HDACs were optimized using GROMOS 96.1 (43A2) force field within GROMACS 4.5 software package<sup>19</sup>. The complete

protein structures were enclosed in cubic box of 4.0 Å edge lengths. This cubic box was solvated with water model and Cl<sup>-</sup> ions were added for charge neutralization. The solvated box were subjected to energy minimization of steepest decent for maximum force of <1000.0 kJ/ mol. The optimized structures of HDACs were subjected to molecular docking study.

The ligands included in the docking analysis were TSA, SFN and TQ. The 3D coordinates of these ligands were obtained from ChEBI database ([www.ebi.ac.uk/chebi](http://www.ebi.ac.uk/chebi)) (Figure 1). These ligands hold the CHEBI identification number of 46024, 4807 and 19371, respectively.

### 2.1.3. Autodock

Molecular docking study was carried out with the help of automated docking program, Autodock 4.0<sup>20</sup>. Docking analysis was based upon Lamarckian Genetic Algorithm (LGA) and population size of 150 combinations was considered for grid-energy evaluation and generation of grid maps. In the preliminary step of protein preparation, the associated water molecules were removed and structure containing single conformation was taken for further study. Autogrid was set at docking area for all ligands at grid points of 0.37 Å. The similar structures were grouped into one cluster on the basis of root mean square deviation (RMSD) and orientation. The docking energy was computed as the sum of intermolecular and the internal energies. In the final instance, the best orientation or the pose with the lowest estimated energy ( $\Delta G$ ) were chosen from each cluster.

### 2.1.4. Molecular Dynamics (MD) Simulations

In order to study the stability of the docked conformation, molecular dynamics study was carried with the help of GROMACS 4.5.4 package using GROMOS96 43a1 force field. The docked complex having lowest binding energy was subjected to MD simulation study. The protein topology parameter was assigned based upon gromacs force field while ligand topology details were generated by using Dundee PRODRG server<sup>21</sup>. HDAC-inhibitor complexes were placed in the cubic box of simple point charge water molecule. Overall

system containing HDAC-inhibitor complex was neutralized by adding Cl<sup>-</sup> ion. The energy minimization was carried out by following steepest descent and conjugate gradient method in order to release conflicting contacts. The step for energy minimization was followed by equilibration of the system. The complete system protein-inhibitor complex, counter ions and water molecule were subjected to the position-restrained dynamics simulation (NVT and NPT) at 300K for 100ps. Finally the system was subjected to production run at 300 K temperature and 1 bar pressure for 5000 ps. The co-ordinates of each atom was recorded at every 100ps during MD simulation analysis of the trajectory.

### ***In-vitro* Cell Culture Analyses**

#### **2.1.5. Reagents**

Stock solutions of trichostatin A (TSA), sulforaphane (SFN) and thymoquinone (TQ) (Sigma–Aldrich, St. Louis, MO, USA) were prepared in dimethylsulphoxide (DMSO) (Sigma–Aldrich, St. Louis, MO, USA), stored at -20°C and diluted in fresh medium just before use. Real time PCR primers of p21, Maspin, BAX and BCL2 were obtained from Sigma–Aldrich, St. Louis, MO, USA. For western blot analysis, following antibodies were used: rabbit polyclonal anti-p21, rabbit polyclonal anti-Bax, rabbit polyclonal anti-Bcl2, mouse monoclonal anti-beta actin (Santa Cruz Biotechnology, Santa Cruz, CA, USA). For immunofluorescence, rabbit polyclonal anti-p21 (Santa Cruz Biotechnology, Santa Cruz, CA, USA) was used.

#### **2.1.6. Cell Culture**

Human breast cancer cell line MCF7 and normal human keratinocytes HaCat were procured from National Centre for Cell Science (NCCS), Pune, India and were cultured in Minimum Essential Eagle's Medium (MEM) and Dulbecco's Modified Eagle Medium (DMEM) supplemented with 10% (v/v) Fetal Bovine Serum (FBS, Invitrogen) and 100 IU/mL Penicillin and 0.1 mg/mL streptomycin in a humidified atmosphere of 5% CO<sub>2</sub> at 37°C.

The cells were harvested by trypsinization and the number of living cells was calculated by Trypan blue staining (0.2% v/v) using haemocytometer.

#### **2.1.7. HDAC Activity Assay**

Total HDAC activity was quantified using commercially available colorimetric HDAC Activity Assay Kit (BioVision, Mountain View, CA) as per the manufacturer's instructions. In brief, MCF-7 cells exposed to TSA and SFN for 24 h and TQ for 24, 48, 72 h were harvested to prepare whole cell lysate using RIPA buffer (Sigma–Aldrich, St. Louis, MO, USA). Extracts having 100 µg proteins from vehicle (DMSO) and drug treated cells were incubated with 10 µl 10X HDAC buffer and 5 µl acetylated lysine side chain containing HDAC colorimetric substrate for 3 h at 37°C to initiate the HDAC reaction. Lysine developer was then added, and the mixture was incubated for 30 min at 37°C. The chromophore was then measured using micro-plate reader spectrophotometer (Perkin-Elmer, Waltham, MA, USA) at 405 nm. The colorimetric signal produced is directly proportional to HDAC activity.

#### **2.1.8. Total RNA extraction and analysis of mRNA Expression**

The MCF-7 breast cancer cells were treated with TSA, SFN and TQ at their respective IC<sub>50</sub> for 24 h. Total RNA was then extracted with TriReagent (Sigma–Aldrich, St. Louis, MO, USA) according to the manufacturer's recommendations. After that, total RNA (1µg) was reverse-transcribed with oligodT using the RevertAid First Strand cDNA Synthesis Kit (Thermo Scientific). Quantitative reverse transcription PCR (qRT-PCR) was performed with a Realplex4 Eppendorf system using SYBR® Green JumpStart™ Taq ReadyMix. After an initial denaturation step at 95 °C for 6 min, 40 cycles were performed including a denaturation step at 95 °C for 15 s, annealing at 53 °C (p21, Maspin) and 59.8 °C (Bax, Bcl2) for 30 s, and extension at 72 °C for 60 s. GAPDH amplification was used as a qualitative control. The primer sequences for qRT-PCR analysis of p21, Maspin, Bax, Bcl2 and GAPDH genes were given in Table 1.

### 2.1.9. Protein extraction and Western Blot Analysis

80–85% confluent MCF-7 cells were used to prepare cell lysates using RIPA buffer (50 mM Tris-HCl (pH 8.0), 150 mM NaCl, 0.5% sodium deoxycholate, 1% NP40 and 0.1% sodium dodecyl sulfate) supplemented with a protease inhibitor cocktail (Sigma–Aldrich, St. Louis, MO, USA) as described previously<sup>22</sup>. Protein concentration in the supernatants was estimated by Bradford method. Aliquots (50 µg) of total proteins were subjected to electrophoresis through a 12% SDS-polyacrylamide gel at a constant voltage of 120 V in running buffer. Resolved proteins were then transferred to PVDF membranes (Millipore). The protein containing membranes were blocked with 3% Bovine Serum Albumin (BSA) in Phosphate buffer saline containing 0.1% Tween-20 (PBST) for 2 h. Immunostaining was carried out using primary antibody incubation overnight. The blots were then subjected to washing and incubated with appropriate secondary antibody coupled to horseradish peroxidase (HRP). The SuperSignal West Femto Chemiluminescent Substrate (Thermo Scientific) was used for visualization of the secondary antibody. The signals from the blots were scanned using the Gel Documentation system (Bio-Rad) and analyzed by Image J software. Beta actin was used to confirm equal protein loading.

### 2.1.10. Immunofluorescence Microscopy

MCF-7 breast cancer cells were plated on sterilized glass coverslips in 6-well dishes and treated with TSA, SFN and TQ at their respective IC<sub>50</sub> for 24 h. The cells were then fixed in ice cold methanol and were permeabilized by 0.25% Triton X-100 in phosphate buffered saline (PBST). After blocking in 1% BSA in PBST for 30 min, the cells were incubated overnight at 4°C in primary antibodies (1:100 dilution in phosphate-buffered saline, 1% bovine serum albumin for all antibodies). The cells were rinsed with PBS then incubated with FITC-conjugated goat anti-rabbit secondary antibody (Santa Cruz Biotech).

### 2.1.11. Cell-cycle Analysis

MCF-7 cells were plated at  $5 \times 10^5$  cells/60-mm dish. The cells were treated with TSA, SFN and TQ at their respective doses for 24 h. After the treatment, cells were harvested by trypsinization and fixed in 70% ethanol. The cells were then collected by centrifugation at  $600 \times g$  for 5 min at  $4^\circ C$  and washed twice with PBS. This was followed by resuspension of cells in PBS containing 250 U/ml RNase for 20 min at room temperature and staining with  $100 \mu g/ml$  propidium iodide (PI). The DNA content was examined with FACS Aria (Becton Dickinson, San Jose, CA, USA). Cell-cycle distribution was analyzed using FlowJo (Becton Dickinson) software.

#### **2.1.12. Evaluation of cytotoxicity of TSA, SFN and TQ by MTT assay**

The MTT (3-(4,5-dimethylthiazol-2-yl)-2,5-diphenyltetrazolium bromide) assay is a colorimetric detection method. It is a sensitive measure of cytotoxic effects induced by cancer chemotherapeutic drugs in vitro condition. MCF7 and HaCat cells (80 % confluent) were seeded into a 96 well culture plates ( $8 \times 10^3$  cells/well for MCF-7 and  $5 \times 10^3$  cells/well for HaCat). The drugs TSA (25-200 nM), SFN (1-25  $\mu M$ ) and TQ (10-50  $\mu M$ ) were then subjected to both cell lines. After 24 hours of drug treatment, 100  $\mu l$  of MTT solution (0.8 mg/ml, diluted in serum free culture medium) were added and allowed to incubate for 4 hours in dark at  $37^\circ C$ . The black formazans formed were dissolved with DMSO and allowed to incubate for 15 minutes in dark. The absorbance was measured at 570nm by micro-plate reader spectrophotometer (Perkin-Elmer, Waltham, MA, USA) and the results were expressed as the mean of three replicates as a percentage of control (taken as 100%).

#### **2.1.13. Cell morphology and imaging**

MCF7 cells in logarithmic growth phase were seeded at  $3 \times 10^5$  cells/ml and treated with TSA, SFN and TQ at their sub-lethal concentration ( $IC_{50}$ ), in control group added DMSO (0.01%), and incubated for 24h. Cell morphology was observed and phase contrast images of cells were taken by inverted microscope (Olympus IX71, USA).

#### **2.1.14. Chromatin Condensation Assay**

For chromatin condensation assay, MCF-7 and HaCat cells ( $10^5$  Cells/well) were seeded in 6 well culture plates and allowed to grow for one day. Then cells were treated with drugs (TSA, SFN and TQ) at their respective  $IC_{50}$  values for 24 h. The cells were stained with Hoechst 33342 dye and images were taken under UV filter using Epi-fluorescent microscope (Olympus IX71, USA) at 400 X magnification. Condensed nuclei were counted against total number of nuclei in the field, and the percentage of apoptotic nuclei were calculated and plotted graphically.

#### **2.1.15. Measurement of DNA Damage by Comet Assay**

Comet assays were performed under alkaline conditions to determine the amount of double-strand DNA breaks. MCF-7 cells and HaCat cells were subjected to treatment with TSA, SFN and TQ at their respective  $IC_{50}$  values for 24 h. Then cells were harvested and added to preheated ( $37^{\circ}C$ ) low-melting point agarose. The solution was pipetted onto slides precoated with 1% agarose. The slides were allowed to lyse overnight at  $4^{\circ}C$  in alkaline lysis solution (1.2 M NaCl, 100 mM Na<sub>2</sub>EDTA, 0.1% sodium lauryl sarcosinate, 0.26 M NaOH, pH > 13) prior to immersion in alkaline electrophoresis solution (0.03 M NaOH, 2 mM Na<sub>2</sub>EDTA, pH ~12.3). After 30 min, slides were placed into a horizontal electrophoresis chamber samples for 25 min (0.6 V/cm). The slides were washed with deionized H<sub>2</sub>O to remove the alkaline buffer, stained with propidium iodide (10  $\mu$ g/ml stock) and incubate for 20 min. The slides were then washed with water and examined by Epi-fluorescent Microscope (Olympus IX71).

#### **2.1.16. Cell migration Analysis by Wound-healing Assay**

MCF-7 cells and HaCat cells were seeded to form a nearly confluent cell monolayer on the culture surface. Wounds were then made by using sterile 200  $\mu$ l pipette tips and the cell debris was removed by washing with PBS. The wounded cell monolayer was then

incubated with TSA, SFN and TQ at their respective IC<sub>50</sub> values. After the wound in the control was healed up the photographs were taken.

### 2.1.17. Clonogenic Assay

MCF-7 cells and HaCat cells were plated at a low density (500 cells/well) in a 6 well plate, allowed to attach for 24 hours prior to treating with the drugs. Then cells were treated with TSA, SFN and TQ at their respective doses. Cells were grown until distinct colonies were formed in untreated controls. Then they were fixed and stained with a mixture of 6.0% glutaraldehyde and 0.5% crystal violet, air dried, photographed and evaluated for colony estimation.

### 2.1.18. Statistical analyses

Statistical analyses of the data were performed by t-test using SPSS software. Differences were analyzed for significance by one way ANOVA with a post hoc Tukey HSD (Honestly Significant Difference) test, which tests each sample against respective control. All data are presented as mean  $\pm$  SD. Variation with  $p < 0.05$  was considered to be significant for all experiments. In case of HDAC activity, variation with  $p < 0.01$  and  $p < 0.05$  were considered to be significant.

## 3. Results:

### 3.1. *In-silico investigations:*

#### 3.1.1. HDAC1 and HDAC2 establish homology with *Aquifex aeolicus*

The homology in the deacetylase domain for human HDAC1 and HDAC2 proteins was established with the model organism *Aquifex aeolicus*. In figure 2, the highlighted regions in blue exhibit the presence of conserved domain between the HDAC proteins and the model organism. The amino-acid sequence highlighted in yellow displays the existence of similar amino acid in the domain. Owing to the higher homology with the model organism, human HDAC1 and HDAC2 proteins were considered for further interrogation in our study.

### 3.1.2. Molecular interaction and Binding energy of TQ with HDAC1 and HDAC2

Each classical HDAC shares a common deacetylase domain of approximately 390 amino acids constituting the catalytic site. A narrow cylindrical structure of a length equivalent to that of a 4–6 carbon straight chain with a  $Zn^{2+}$  near its base, forms the enzyme pocket of the catalytic domain. The inhibitory potential of TQ was analyzed at  $Zn^{2+}$  binding site of HDAC catalytic pocket<sup>23</sup>. The interaction for TQ was evaluated in reference to TSA and SFN, the two well-known HDAC inhibitors. The binding energy was calculated based upon intermolecular and torsional free energy and the best possible orientation of the ligand was identified. In an interaction with HDAC1 (4BKX) enzyme, 100% conformation of TQ showed an average binding energy of -6.98 kcal/mol. In contrary, only 50% of the total conformation of TSA bound to active site pocket with an average binding energy of -7.2 kcal/mol (Figure 3, panel [I] c). Similarly, 80% conformation of TQ holds mean binding energy of -7.2 kcal/mol, while only 55% of TSA interacts with the active site pocket of HDAC2 (3MAX) enzyme with binding energy of -9.2 kcal/mol (Figure 2, panel [II] c). The binding energy of SFN is comparatively less than TQ and TSA (Table 1). The elevation in average binding energy is characterized by non-covalent interactions, mainly electrostatic, hydrogen bonding and the van der Waals interactions. While TSA establishes an average of 7 hydrogen bonds with HDAC1, the higher binding energy with HDAC2 protein owes to its non-covalent interaction of hydrogen bonding, electrostatic and van-der Waals interaction. TQ interacts via 3 hydrogen bonds in the active site pocket of both HDAC1 and HDAC2. SFN holds lesser binding due to distant association of hydrogen bonds and the van-der Waal interaction. Histidine and aspartate amino residue are identified to actively participate in the interaction. The detailed molecular interaction of the inhibitors with the respective HDACs can be visualized in figure 3, panel [I] [II] b. Owing to detailed study of enzyme-inhibitor

complexes (Figure 3, panel [I] [II] a), the stability of complexes was predicted based upon molecular dynamics simulation studies.

### 3.1.3. Characterization of stability of HDAC-inhibitor complexes by MD simulation

The molecular dynamics simulation study was carried out to investigate the dynamic behaviour of the ligands (TSA, SFN and TQ) within the pocket of receptor HDAC and to predict the most reliable receptor-ligand interaction mechanism. The stability of the docked conformation was analysed with respect to root mean square deviation (RMSD) and average hydrogen-bonding between HDAC-inhibitor complexes. Overall, HDAC1-inhibitor complexes remained stable up to 2ns, while the mean fluctuation of 2.14 Å and 2.43 Å was observed when TSA and TQ interacts HDAC1 protein. Similarly, TSA and TQ on interaction with HDAC2 attain equilibrium with an average fluctuation of 2.06 and 2.55 Å. When SFN interacts with HDAC proteins, average deviation of 2.74 and 2.75 Å is attained by the respective protein backbone (Figure 4) (Table 2). Thus, from the findings, it can be inferred that TQ holds similar stability with HDACs as that of SFN.

The stability of the HDAC-inhibitor complexes were also characterised by the binding mode of inhibitors (TSA, SFN and TQ) inside the active site pocket. An average hydrogen bond formation was estimated between HDAC-inhibitor complexes. It is evident from our investigation that TQ forms higher number of hydrogen bond with the cognate donor/receptor in proximity of active site pocket of HDAC enzyme. On average 3.47 and 5.2 hydrogen bonds are formed when TSA makes complex with HDAC1 and HDAC2, respectively. Similarly, TQ interacts with the respective protein by average hydrogen bonds of 2.35 and 2.5. SFN also holds similar mode of interaction as that of TQ (Figure S1) (Table 2).

Thus, MD simulation studies based upon RMSD and average hydrogen bonding affirm that the stability of HDACs-TQ complex is similar to that of SFN. Further ahead, the

*in-vitro* characterization was carried out to unravel the ability of TQ in HDAC inhibition and successfully restore the expression of tumor suppressor genes.

### **3.2. *In-vitro* analyses:**

#### **3.2.1. TQ inhibits HDAC activity in MCF-7 breast cancer cells**

The well-established HDAC inhibitors including TSA, butyrate and SFN modulate histone acetylation level by inhibiting activity of HDAC. To examine whether TQ has any role in HDAC inhibition, we analyzed TQ treated MCF7 cells for *in-vitro* HDAC activity. Corroborating our *in-silico* findings, TQ was observed to exhibit HDAC inhibition at its IC<sub>50</sub> (34 μM) in a time dependent manner. MCF-7 cells treated with TQ for 24 h were shown to attenuate HDAC activity compared to control at a significant level of p<0.05. However, drastic change in HDAC activity is observed post-treatment with TQ for 48 and 72 h. TSA and SFN exhibit similar change in HDAC activity on treatment for 24 h. This change in enzyme activity is found to be significant at p-value < 0.01 (Figure 5).

#### **3.2.2. Expression Analysis of HDAC target and apoptosis related genes (p21, Maspin, Bax and Bcl2)**

The cell cycle regulatory gene, p21waf1/cip1 and anti-cell proliferative and apoptosis inducing gene, Maspin have been shown to be epigenetically governed via histone acetylation<sup>24, 25</sup>. It has been widely reported that the promoter region of p21waf1/cip1 is negatively controlled by HDAC recruited at its Sp1 sites<sup>1, 26</sup>. According to Juan et al, HDAC regulates the acetylation status of p53 which in turn, results in decrease expression of Bax. However, in presence of HDAC inhibitor Bax is overexpressed<sup>27</sup>. Hence, it is hypothesized that TQ induces transcription at p21, Maspin and Bax promoter through down-regulation of HDAC activity similar to other HDAC inhibitor. To examine this, we executed quantitative RT PCR and Western blot analyses. As expected, we found the increased transcript level of p21, Maspin and Bax in TQ treated MCF-7 cells (Figure 6). Result obtained from western

blot and immunofluorescence microscopy also clearly demonstrated the role of TQ in promoting the expression of p21 at protein level (Figure 7 and 8). Moreover, TQ treatment promoted the pro-apoptotic Bax expression, while attenuated the anti-apoptotic Bcl-2 expression, at both transcript and protein level compared to control (Figure 6 and 7).

In addition, HDAC inhibitor dependent increased expression of p21 can also arrest cell cycle at G1 and/or G2 phase.

### **3.2.3. TQ arrests G2/M phase of cell cycle**

HDAC inhibitors, including SFN have been demonstrated to disrupt checkpoints during G2/M phase of cell cycle<sup>28</sup>. In view of this, the effect of TSA, SFN and TQ on breast cancer cell cycle distribution was analyzed by FACS. It is observed that the percentage of cells in G2M phase reached a value of 33.2% after 48 h exposure to TQ, which is nearly equal to that of TSA (33.9 %) with respect to control (17.7%) (Figure 9). This substantiates the active role of TQ in HDAC inhibition.

Further, in the upcoming analyses, we have demonstrated the cytotoxic effect of TQ in metastatic breast adenocarcinoma MCF-7 cells.

### **3.2.4. TQ treatments alters cancer cell morphology**

HDACs are important regulators of cell proliferation and differentiation. Interestingly, phase-contrast light microscopy reveals that TQ treatment of MCF-7 cells changed their morphology. Generally, untreated MCF-7 cells have slightly polygonal and cobblestone-like phenotype. Following incubation with different HDAC inhibitors, the cells undergo distinct morphological changes. In TSA treatment, the cells underwent shrinkage with prominent extensions, while SFN had no considerable phenotypic alterations. Intriguingly, TQ leads to the formation of cytoplasmic vacuoles and rounding of cells in MCF-7 cells (Figure S2 A) in contrast to normal cells (HaCat) (Figure S2 B). Moreover, decreased cell number and the appearance of floating cells revealed the cytotoxic effect of TQ to MCF-7 cells.

### **3.2.5. TQ exerts higher cytotoxic effect on breast cancer cells than normal cells**

The cytotoxic property of TSA, SFN and TQ was examined in breast cancer cells as well as in normal keratinocytes (HaCat). A remarkable decline in cell viability was noticed with increasing concentration of these drugs in MCF-7 cells. Fortunately, in case of normal cells TQ elicits no lethal effect as that of TSA and almost all cells were remained viable even at 100 $\mu$ M TQ. For MCF-7 cells, the sub-lethal concentration ( $IC_{50}$ ) of TSA, SFN and TQ was identified to be 180nM, 10 $\mu$ M and 34 $\mu$ M, respectively. Of note, we observed that SFN at its  $IC_{50}$  has some cytotoxic effect on normal cells, while for TQ there was no trace of such effect (Figure S3).

### **3.2.6. TQ induces chromatin condensation and DNA damage in breast cancer cells**

Chromatin condensation assay aids in determining the cell death inducing ability of drug, which is indicated by formation of highly condensed and fragmented apoptotic bodies. The number of condensed nuclei in TQ is found to be almost similar to that of SFN in MCF-7 cells in contrast to untreated cells (Figure S4). Moreover, the non-toxic effect of TQ towards normal cell is clearly visible due to least number of condensed nuclei in comparison to TSA.

Further, comet assay indicates the extent of DNA damage due to apoptosis on application of any insults to the cells. The tail length denotes the apoptosis inducing ability of drugs. The increased tail length is observed in TQ treated MCF-7 cells similar to TSA and SFN. Conversely, in normal cells TQ induces less DNA damage, as revealed by the short tail length (Figure S5).

### **3.2.7. TQ inhibits migration and proliferation of breast cancer cells**

The cytotoxic property of the inhibitors is also characterized by its anti-migratory and anti-proliferative potency. In view of this we have seen that TQ holds considerable efficiency to inhibit the migration of MCF-7 cells similar to that of TSA and SFN. In contrary, it does not affect the migration of normal cells (Figure S6).

Similarly, the clonogenic assay reveals the anti-proliferative effect of TQ in MCF-7 cells. It has been observed that TQ effectively inhibits the proliferation of MCF-7 cell, while it is non-effective to normal cell. This is clearly revealed by comparatively less number of colonies formed in MCF-7 than the HaCaT cells (Figure S7).

Based upon the above findings it is evident that TQ is non-toxic to normal cells and can be successfully implemented clinical applications.

#### 4. Discussion and Conclusion:

DNA methylation mediated gene silencing is invariably associated with histone deacetylase activity<sup>29, 30</sup>. The recognition that HDACs are causally implicated in cancer has exhilarated the development of small-molecule inhibitors as anticancer drugs. Despite identification of structurally diverse classes of HDAC inhibitors, several of them hold considerable toxicity, unintended off-target effects and poor bioavailability leading to their limited therapeutic implications<sup>31</sup>. This led us to explore the possible role of most commonly consumed dietary phytochemical, thymoquinone (TQ) in HDAC inhibition. Previous studies have explored the anticancer activity of TQ by p53-dependent and independent apoptosis, involving induction of PPAR- $\gamma$  (peroxisome proliferator-activated receptor gamma), PTEN (Phosphatidylinositol 3,4,5-trisphosphate 3-phosphatase), NF- $\kappa$ B and AKT<sup>9, 10, 16, 32, 33</sup>. Gurung et al explained the anticancer effect of TQ in terms of its ability to induce DNA damage and telomere attrition, by inhibiting telomerase and cell death<sup>34</sup>. However, the molecular mechanism of TQ induced growth inhibition and pro-apoptotic effects in cancer is still at its infancy<sup>14, 34</sup>. The present investigation, for the first time, illustrates the plausible insight into this question by demonstrating that TQ inhibits HDAC activity in human breast adenocarcinoma MCF-7 cells.

We initiated our investigation with an *in-silico* approach using docking analyses followed by molecular dynamic (MD) simulation study. Known inhibitors of HDACs, TSA

and SFN are considered as reference molecule in our analyses. Higher binding affinity of TQ with HDAC1 and HDAC2 compared to SFN and apparently similar to that of TSA reveals its potential to inhibit HDACs (Figure 3, panel [I] [II] c). Furthermore, the stability of TQ inside the binding pocket of HDACs has been validated by RMSD and average hydrogen bonding (Figure 4, S1). Formation of such stable complex is also underpinned by the fact that TQ undergo covalent bond formation with the nucleophilic amino acid side chains of Cys and His residues. It occurs through a highly reactive  $\alpha$ ,  $\beta$ -unsaturated carbonyl group (a Michael acceptor) of TQ<sup>35, 36</sup>. This clearly elucidates that TQ forms stable and energetically favored complex with HDACs. Such property of TQ can be successfully employed in the development of irreversible drugs for the treatment of cancer<sup>37</sup>. Corroborating our *in-silico* findings, the *in-vitro* examination explicates the potential role of TQ in HDAC inhibition. Generally, enhanced expression of HDACs has been reported in various cancers<sup>38</sup> and inhibitors have been identified to successfully impede their activity<sup>1, 23</sup>. Previously, the phytochemicals, such as butyrate and SFN are known to inhibit enzymatic activity of HDAC<sup>2</sup>. Intriguingly, our study has revealed TQ as a potential candidate that ameliorated total cellular HDAC activity in MCF-7 cells in time dependent manner. Our observation that TQ is capable of decreasing HDAC activity in treated cells is consistent with the existing HDAC inhibitors (Figure 5). This finding is further substantiated by the enhanced expression of HDAC target genes on application of TQ. Previous reports have shown that p21 promoter is epigenetically repressed by HDAC activity via their Sp1 sites and HDAC inhibitors, such as TSA, apicidin, phenylbutyrate, SAHA and *Helminthosporium carbonum* toxin could induce p21 expression in MCF-7 cells<sup>1, 26, 39</sup>. Similarly, histone hypoacetylation mediated epigenetic silencing of maspin can be successfully reversed by TSA in MCF-7 cells<sup>25</sup>. In agreement with this, we observed that TQ markedly enhanced the expression of p21 and Maspin both at transcript and protein level. Moreover, we demonstrated that the ability of TQ to restore the

expression of these HDAC target genes is almost similar as that in TSA and SFN treatment. As previously seen by other groups, it was found that on treatment with known HDAC inhibitors (TSA and SFN), the expression of pro-apoptotic Bax expression is upregulated and that of anti-apoptotic Bcl-2 is down-regulated<sup>40, 41</sup>. Consistent expression profile of Bax and Bcl-2 was observed in case of TQ treated MCF-7 cells (Figure 6-8). The differential expression profile of the HDAC target and apoptosis related genes are the universal consequences of downstream effects of HDAC inhibitor. In our investigation, TQ elicits similar expression profile; this apparently reflects the HDAC inhibition potential of TQ.

To further support our findings, we analyzed the cell cycle progression in the MCF-7 cells treated with TSA, SFN and TQ. In harmony with HDAC inhibitor's previously reported G2/M phase arrest in cancer cells<sup>42, 43</sup>, we found increased percentage of cells in G2/M interface following TSA, SFN and TQ treatment, compared to untreated control (Figure 9). It is well known that the p21 is implicated in inducing G1/S phase arrest through its interactions with cyclin E/cdk2, however, in p53 wild type cells, such as the LnCaP prostate cancer cells, p21 induction by HDAC inhibitor has also been demonstrated to induce G2/M arrest<sup>43</sup>. Collectively, TQ mediated HDAC activity attenuation leads to p21 induction, which in turn arrest the MCF-7 cells in G2/M interface ultimately resulting in reduced cell proliferation.

Identification of HDAC inhibitor with high therapeutic efficacy and minimal cytotoxicity continues to be an unmet challenge. In a quest to address this, after unraveling the role of TQ in HDAC inhibition, our next attempt was to inspect its cytotoxic nature towards normal cells. TQ, at its sub-lethal concentration ( $IC_{50}$  34  $\mu$ M) induces formation of cytoplasmic vacuoles in MCF-7 breast cancer cells, while HaCat cells exhibit no obvious abnormality (Figure S2). This may stem from cytotoxic property of TQ, as shown previously by Rachoma et al in glioblastoma cells<sup>44</sup>. It is also apparent from cytotoxic MTT assay that TQ, unlike TSA possess no cytotoxic effect in normal HaCat cells, while it exerts extensive

toxic effect to MCF-7 cells (Figure S3). Supporting these findings, in normal cells, TQ was found to induce less condensed chromatin and DNA damage (Figure S4, S5), which are hall marks of apoptosis. In agreement with this finding, TQ was also demonstrated to exert less anti-proliferative and anti-migratory effect in HaCat cells compared to MCF-7 cells (Figure S6, S7). Thus, our findings well illustrate that TQ exhibits specific cytotoxicity in MCF-7 cells, while eliciting no such effect in normal cells.

In conclusion, this investigation reveals a new role of TQ in inducing anticancer threat on metastatic breast adenocarcinoma cells via attenuation of global HDAC activity, ensuing prevalent epigenetic changes. Indeed, such changes are implicated in the regulation of genes, including p21, maspin, Bax and Bcl-2 and eventually eliciting strong anticancer effect. Moreover, TQ is a natural dietary component with no obvious cytotoxicity to normal cells. In line with this, further investigation may be executed in experimental models and clinical settings to enlist TQ as a chemo-preventive drug, which may lead to a durable cure for breast cancer.

**Notes:** The authors declare no competing financial interest.

#### References:

1. M. A. Gluzak and E. Seto, *Oncogene*, 2007, **26**, 5420-5432.
2. M. C. Myzak and R. H. Dashwood, *Curr Drug Targets*, 2006, **7**, 443-452.
3. M. Dokmanovic, C. Clarke and P. A. Marks, *Molecular cancer research : MCR*, 2007, **5**, 981-989.
4. N. Azad, C. A. Zahnow, C. M. Rudin and S. B. Baylin, *Nature reviews. Clinical oncology*, 2013, **10**, 256-266.
5. A. A. Lane and B. A. Chabner, *Journal of clinical oncology : official journal of the American Society of Clinical Oncology*, 2009, **27**, 5459-5468.
6. S. Shukla, S. M. Meeran and S. K. Katiyar, *Cancer letters*, 2014, **355**, 9-17.
7. A. Shilpi, S. Parbin, D. Sengupta, S. Kar, M. Deb, S. K. Rath, N. Pradhan, M. Rakshit and S. K. Patra, *Chemico-biological interactions*, 2015, **233**, 122-138.
8. N. Druesne, A. Pagniez, C. Mayeur, M. Thomas, C. Cherbuy, P. H. Duee, P. Martel and C. Chaumontet, *Carcinogenesis*, 2004, **25**, 1227-1236.
9. C. C. Woo, S. Y. Loo, V. Gee, C. W. Yap, G. Sethi, A. P. Kumar and K. H. Tan, *Biochem Pharmacol*, 2011, **82**, 464-475.
10. M. Roepke, A. Diestel, K. Bajbouj, D. Walluscheck, P. Schonfeld, A. Roessner, R. Schneider-Stock and H. Gali-Muhtasib, *Cancer Biol Ther*, 2007, **6**, 160-169.

11. X. Lei, X. Lv, M. Liu, Z. Yang, M. Ji, X. Guo and W. Dong, *Biochemical and biophysical research communications*, 2012, **417**, 864-868.
12. S. Das, K. K. Dey, G. Dey, I. Pal, A. Majumder, S. MaitiChoudhury, S. C. kundu and M. Mandal, *PloS one*, 2012, **7**, e46641.
13. C. C. Woo, A. Hsu, A. P. Kumar, G. Sethi and K. H. Tan, *PloS one*, 2013, **8**, e75356.
14. H. Gali-Muhtasib, M. Ocker, D. Kuester, S. Krueger, Z. El-Hajj, A. Diestel, M. Evert, N. El-Najjar, B. Peters, A. Jurjus, A. Roessner and R. Schneider-Stock, *J Cell Mol Med*, 2008, **12**, 330-342.
15. A. O. Kaseb, K. Chinnakannu, D. Chen, A. Sivanandam, S. Tejwani, M. Menon, Q. P. Dou and G. P. Reddy, *Cancer Res*, 2007, **67**, 7782-7788.
16. S. A. Arafa el, Q. Zhu, Z. I. Shah, G. Wani, B. M. Barakat, I. Racoma, M. A. El-Mahdy and A. A. Wani, *Mutation research*, 2011, **706**, 28-35.
17. Z. Chen, S. Clark, M. Birkeland, C. M. Sung, A. Lago, R. Liu, R. Kirkpatrick, K. Johanson, J. D. Winkler and E. Hu, *Cancer letters*, 2002, **188**, 127-140.
18. H. M. Berman, J. Westbrook, Z. Feng, G. Gilliland, T. N. Bhat, H. Weissig, I. N. Shindyalov and P. E. Bourne, *Nucleic acids research*, 2000, **28**, 235-242.
19. S. Pronk, S. Pall, R. Schulz, P. Larsson, P. Bjelkmar, R. Apostolov, M. R. Shirts, J. C. Smith, P. M. Kasson, D. van der Spoel, B. Hess and E. Lindahl, *Bioinformatics (Oxford, England)*, 2013, **29**, 845-854.
20. G. M. Morris, R. Huey and A. J. Olson, *Current protocols in bioinformatics / editorial board, Andreas D. Baxevanis ... [et al.]*, 2008, **Chapter 8**, Unit 8 14.
21. A. W. Schuttelkopf and D. M. van Aalten, *Acta crystallographica. Section D, Biological crystallography*, 2004, **60**, 1355-1363.
22. M. Deb, D. Sengupta, S. K. Rath, S. Kar, S. Parbin, A. Shilpi, N. Pradhan, S. K. Bhutia, S. Roy and S. K. Patra, *Biochimica et biophysica acta*, 2015, **1852**, 1630-1645.
23. S. Parbin, S. Kar, A. Shilpi, D. Sengupta, M. Deb, S. K. Rath and S. K. Patra, *The journal of histochemistry and cytochemistry : official journal of the Histochemistry Society*, 2014, **62**, 11-33.
24. A. L. Gartel and A. L. Tyner, *Experimental cell research*, 1999, **246**, 280-289.
25. X. H. Liao, Y. Q. Li, N. Wang, L. Zheng, W. J. Xing, D. W. Zhao, T. B. Yan, Y. Wang, L. Y. Liu, X. G. Sun, P. Hu, H. Zhou and T. C. Zhang, *Cellular signalling*, 2014, **26**, 1335-1346.
26. R. Varshochi, F. Halim, A. Sunters, J. P. Alao, P. A. Madureira, S. M. Hart, S. Ali, D. M. Vigushin, R. C. Coombes and E. W. Lam, *The Journal of biological chemistry*, 2005, **280**, 3185-3196.
27. L. J. Juan, W. J. Shia, M. H. Chen, W. M. Yang, E. Seto, Y. S. Lin and C. W. Wu, *The Journal of biological chemistry*, 2000, **275**, 20436-20443.
28. S. V. Singh, A. Herman-Antosiewicz, A. V. Singh, K. L. Lew, S. K. Srivastava, R. Kamath, K. D. Brown, L. Zhang and R. Baskaran, *The Journal of biological chemistry*, 2004, **279**, 25813-25822.
29. S. K. Patra and M. Szyf, *The FEBS journal*, 2008, **275**, 5217-5235.
30. S. Kar, S. Parbin, M. Deb, A. Shilpi, D. Sengupta, S. K. Rath, M. Rakshit, A. Patra and S. K. Patra, *Cellular and molecular life sciences : CMLS*, 2014, **71**, 1017-1032.
31. O. H. Kramer, M. Gottlicher and T. Heinzl, *Trends in endocrinology and metabolism: TEM*, 2001, **12**, 294-300.
32. G. Sethi, K. S. Ahn and B. B. Aggarwal, *Molecular cancer research : MCR*, 2008, **6**, 1059-1070.
33. T. Yi, S. G. Cho, Z. Yi, X. Pang, M. Rodriguez, Y. Wang, G. Sethi, B. B. Aggarwal and M. Liu, *Molecular cancer therapeutics*, 2008, **7**, 1789-1796.

34. R. L. Gurung, S. N. Lim, A. K. Khaw, J. F. Soon, K. Shenoy, S. Mohamed Ali, M. Jayapal, S. Sethu, R. Baskar and M. P. Hande, *PloS one*, 2010, **5**, e12124.
35. J. M. Chalker, G. J. Bernardes, Y. A. Lin and B. G. Davis, *Chemistry, an Asian journal*, 2009, **4**, 630-640.
36. C. Liao, J. E. Park, J. K. Bang, M. C. Nicklaus and K. S. Lee, *ACS medicinal chemistry letters*, 2010, **1**, 110-114.
37. A. Wissner and T. S. Mansour, *Archiv der Pharmazie*, 2008, **341**, 465-477.
38. S. K. Patra, A. Patra and R. Dahiya, *Biochemical and biophysical research communications*, 2001, **287**, 705-713.
39. V. M. Richon, T. W. Sandhoff, R. A. Rifkind and P. A. Marks, *Proceedings of the National Academy of Sciences of the United States of America*, 2000, **97**, 10014-10019.
40. L. Wang, D. Liu, T. Ahmed, F. L. Chung, C. Conaway and J. W. Chiao, *International journal of oncology*, 2004, **24**, 187-192.
41. J. Ma, X. Guo, S. Zhang, H. Liu, J. Lu, Z. Dong, K. Liu and L. Ming, *Molecular medicine reports*, 2015, **11**, 4525-4531.
42. S. J. Jackson and K. W. Singletary, *The Journal of nutrition*, 2004, **134**, 2229-2236.
43. S. Roy, K. Packman, R. Jeffrey and M. Tenniswood, *Cell death and differentiation*, 2005, **12**, 482-491.
44. I. O. Racoma, W. H. Meisen, Q. E. Wang, B. Kaur and A. A. Wani, *PloS one*, 2013, **8**, e72882.

**Legends to the Tables:**

Table 1: Binding energy (kcal/mol) details of HDAC-inhibitor complexes.

Table 2: Molecular dynamics simulation analysis in terms of with root mean square deviation in (Å) and average hydrogen bonding

Table 3: List of sequence and product length of the real-time PCR primers

**Figure legends**

Graphical Abstract:

**Figure 1:** Chemical structures of (A) Trichostatin A, (B) Sulforaphane and (C) Thymoquinone retrieved from CHEBI.

**Figure 2:** Depiction of conserved deacetylase domains among human HDAC proteins (HDAC1 and HDAC2) and with the model organism, *Aquifex aeolicus* (HDACA). Blue highlighted regions are conserved domains along human HDAC1, HDAC2 and HDACA. The amino-acid sequence highlighted in yellow exhibits the existence of similar amino acid in the domain.

**Figure 3:** (A) Molecular interaction of HDAC1 (4BKX) and HDAC2 (3MAX) with known HDAC inhibitors (TSA, SFN) and candidate inhibitor (TQ). (B) Detailed molecular interaction between active site amino acid residues of HDAC 1 and 2 with TSA, SFN and TQ. The hydrogen bonds have been shown by dotted lines. (C) Binding energy analysis of docked complex of HDAC1 and 2 with the respective known and candidate inhibitors.

**Figure 4:** RMSD plot with respect to time in ns on interaction of TSA (orange), SFN (violet) and TQ (green) with, (A) 4BKX and (B) 3MAX in Å. RMSD is calculated for heavy atoms with reference to their respective orientation in the crystal structures. TQ exhibit similar deviation on interaction with HDAC and forms most stable complex as that of SFN.

**Figure 5:** TQ exhibits HDAC inhibition activity in MCF7 cells in a time dependent manner. MCF-7 cells were treated with TQ for 24, 48 and 72 h and with TSA and SFN for 24 h. Whole cell protein lysates were prepared and incubated with the acetylated substrate peptide provided by the manufacturers. Statistical analysis of the data was performed by one way ANOVA with a post hoc Dunnett Multiple Comparisons test, which compares each sample against the control. Data are expressed as mean  $\pm$  S.D., n=3. Single asterisk ( $p < 0.05$ ) and double asterisk ( $p < 0.01$ ) indicate the level of significance.

**Figure 6:** Real time RT-PCR analysis of HDAC target genes (A) p21, Maspin, and apoptosis related genes (B) Bax, Bcl-2 after treatment with TSA, SFN and TQ in MCF-7 cells. The transcript level of p21, Maspin and Bax are upregulated after treatment with TQ as that of

known HDAC inhibitors (TSA and SFN), while Bcl-2 is downregulated. Data are expressed as mean  $\pm$  S.D., n=3, p < 0.05.

**Figure 7:** (A) Western blot analysis of p21, Bax and Bcl-2 in MCF-7 cells treated with TSA, SFN for 24 h and TQ for 48 h. The protein level of p21 and Bax is enhanced after treatment with TQ like the known HDAC inhibitors (TSA and SFN), while Bcl-2 exhibits diminished expression.  $\beta$ -actin was used as internal control to confirm equal protein loading. (B) Histogram depicting integrated density value for different bands obtained from western blot using ImageJ software. Data are expressed as mean  $\pm$  S.D., n=3, p < 0.05.

**Figure 8:** Immunofluorescence microscopy to detect the p21 expression in untreated and TSA, SFN and TQ treated MCF-7 cells. The expression of p21 is enhanced after treatment with TQ. Each of the images is representative of 30 images obtained from three independent experiments.

**Figure 9:** Cell cycle analysis of MCF-7 cells exposed to TSA, SFN for 24 h and TQ for 48 h at their respective IC<sub>50</sub> in parallel with control (DMSO treated) cells. TQ arrests the MCF-7 cells at G2/M interphase of cell cycle like TSA and SFN. Shown are the representative images of two independent experiments.

## TABLES

Protein	Ligand	RMSD (Å)	Average hydrogen bonding
HDAC1 (4BKX)	TSA	2.14	3.47
	TQ	2.43	2.35
	SFN	2.74	2.12
HDAC2 (3MAX)	TSA	2.06	5.2
	TQ	2.55	2.5
	SFN	2.75	2.2

Table 1

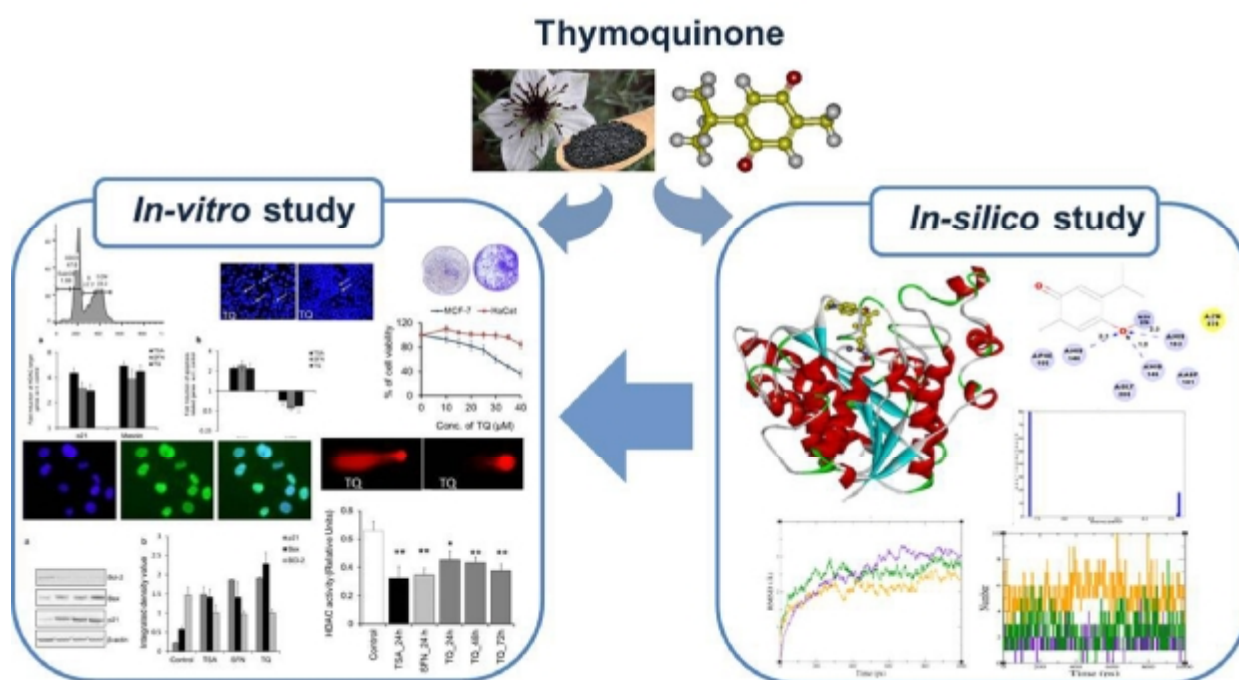
<i>Protein</i>	<i>Ligand</i>	<i>Binding Energy (kcal/mol)</i>
HDAC1 (4BKX)	TSA	-7.2
	TQ	-6.98
	SFN	-5.8
HDAC2 (3MAX)	TSA	-9.2
	TQ	-7.2
	SFN	-5.45

Table 2

Gene	Primer sequence	Amplicon size (bp)
P21	5'-TGAGCCGCGACTGTGATG-3' 5'-GTCTCGGTGACAAAGTCGAAGTT-3'	82
Maspin	5'-GGAATGTCAGAGACCAAGGGA -3' 5'-GGTCAGCATTCAATTCATCCTT-3'	139
Bax	5'-TTCATCCAGGATCGAGCAG-3' 5'-CGCTCAGCTTCTTGGTGG-3'	94
BCI-2	5'-CCTGTGGATGACTGAGTACC-3' 5'-GAGACAGCCAGGAGAAATCA-3'	128
GAPDH	5'-GGAGCGAGATCCCTCCAAAAT-3' 5'-GGCTGTTGTCATACTTCTCATGG-3'	197

Table 3

## FIGURES:



## Graphical Abstract

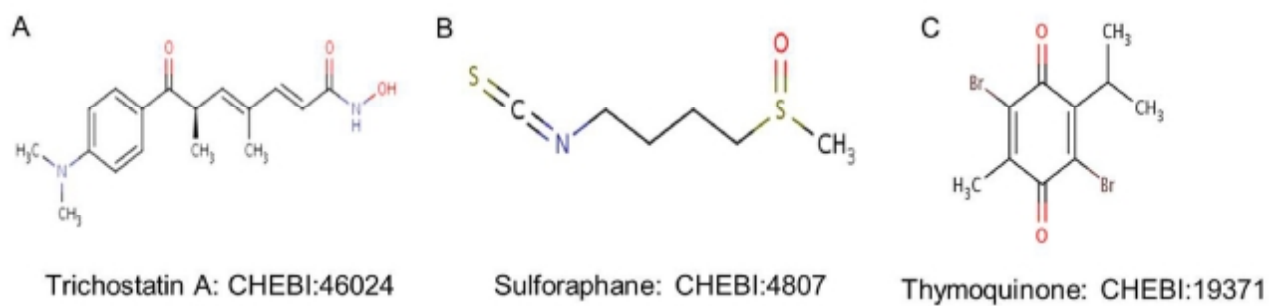


Figure 1

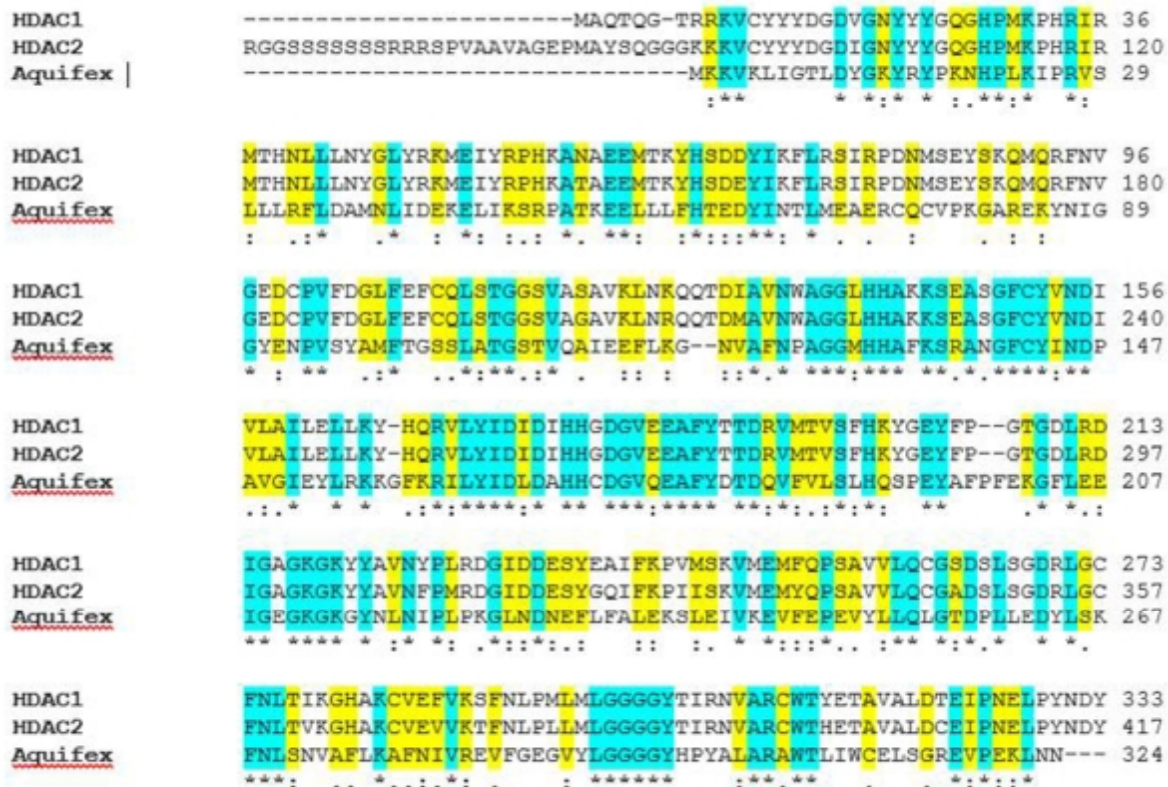
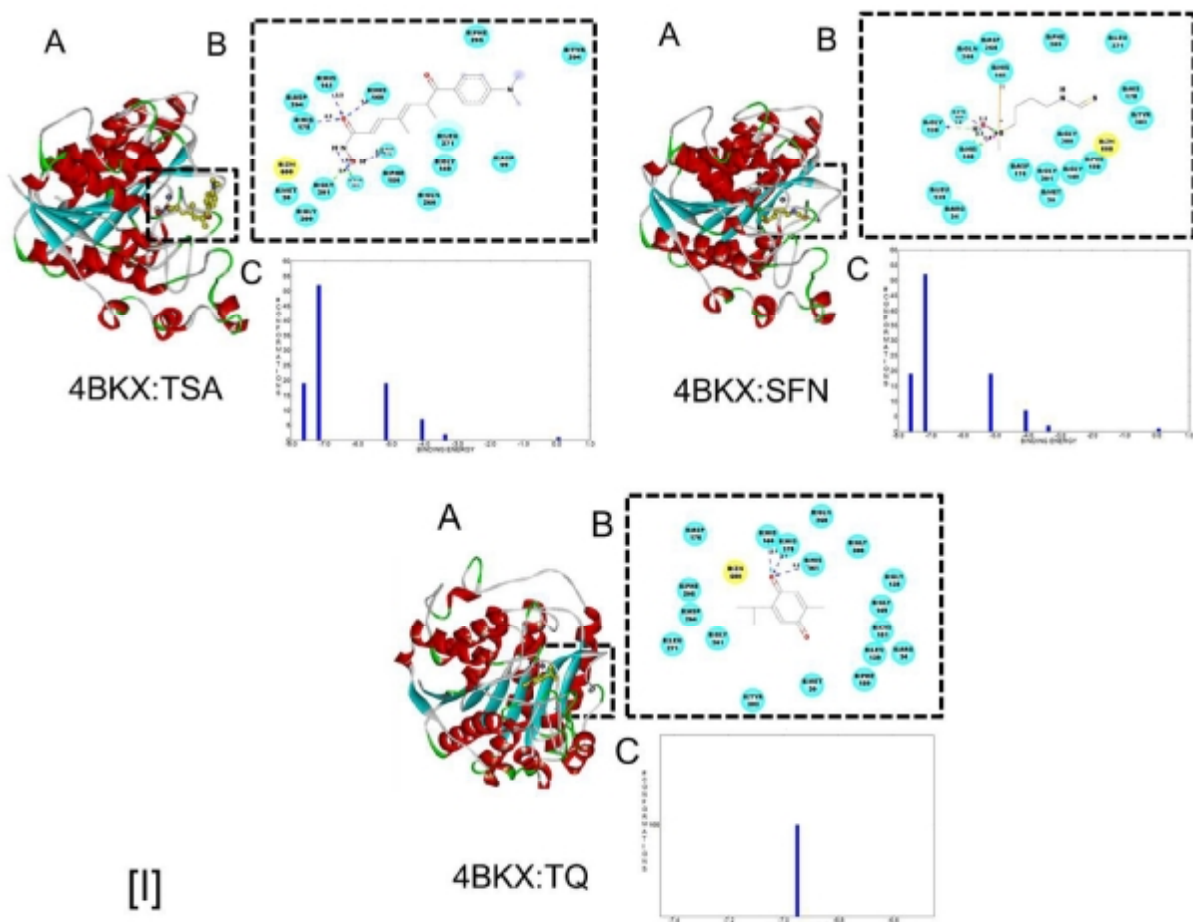


Figure 2



[1]



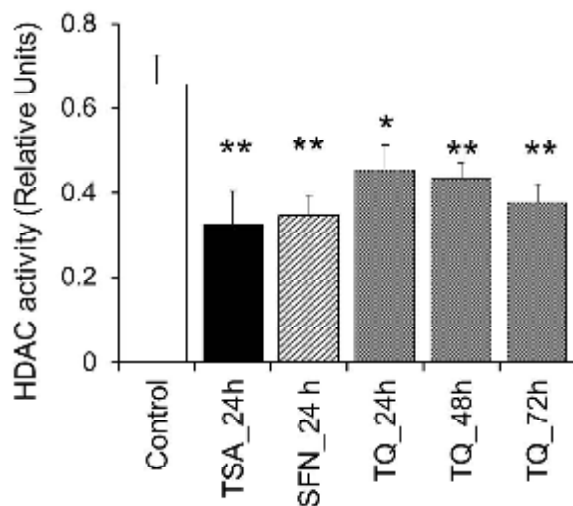


Figure 5

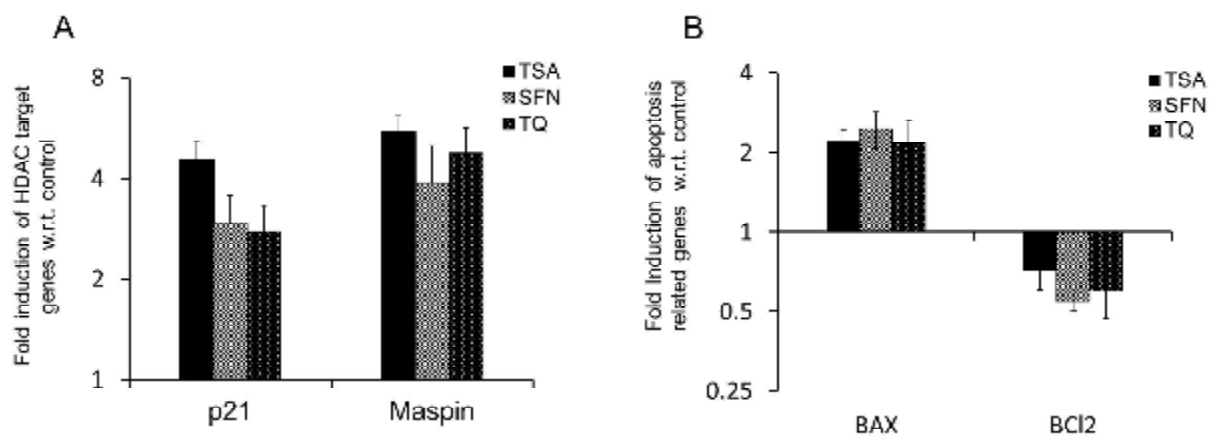


Figure 6

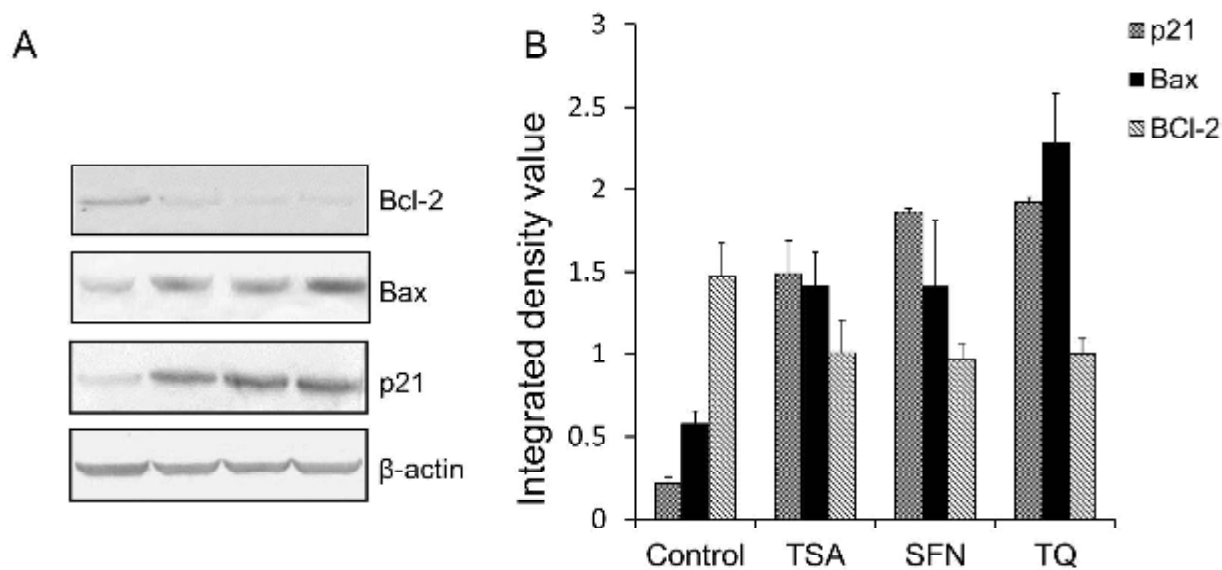


Figure 7

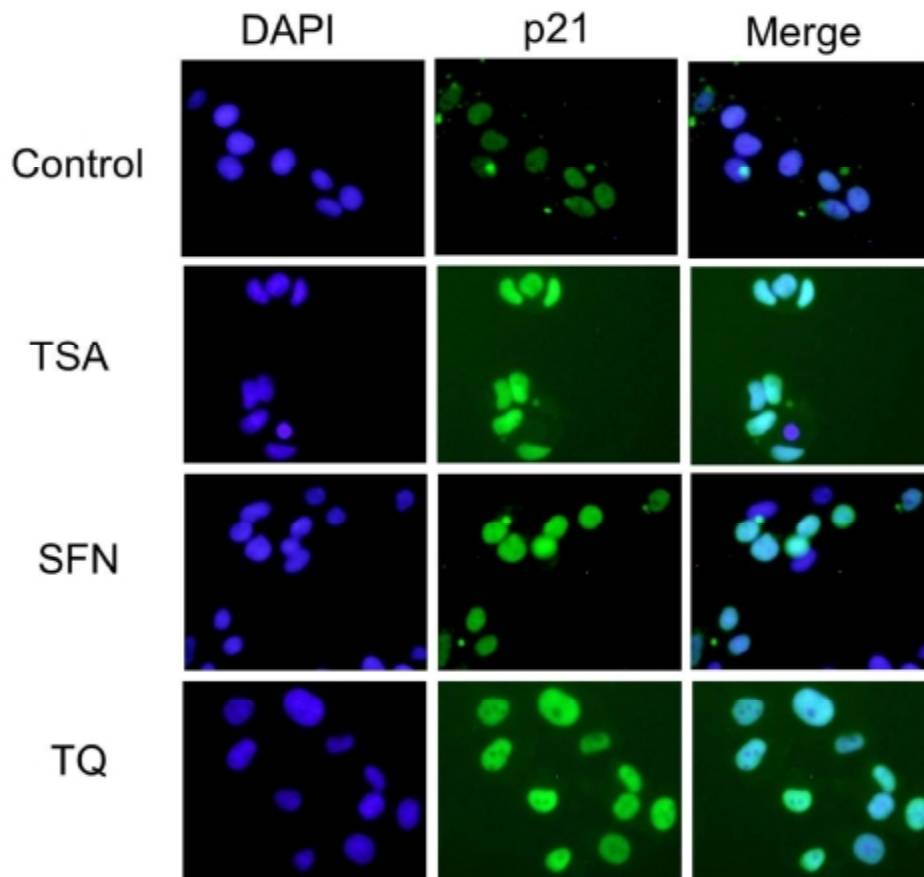


Figure 8

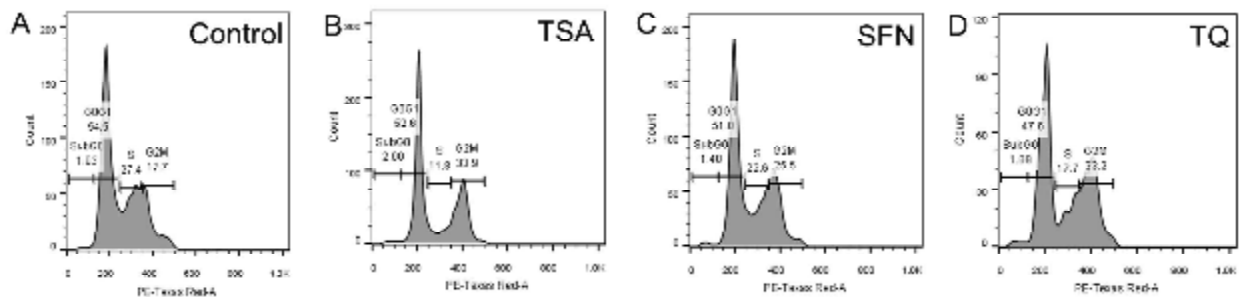


Figure 9